PCCP

PAPER

View Article Online
View Journal | View Issue

Cite this: *Phys. Chem. Chem. Phys.*, 2016, **18**, 30857

RIDME spectroscopy on high-spin Mn^{2+} centers†

D. Akhmetzyanov,‡[a] H. Y. V. Ching,‡[b] V. Denysenkov,[a] P. Demay-Drouhard,[cd] H. C. Bertrand,[cd] L. C. Tabares,[b] C. Policar,[cd] T. F. Prisner*[a] and S. Un*[b]

Received 28th July 2016,
Accepted 5th October 2016

DOI: 10.1039/c6cp05239h

www.rsc.org/pccp

Pulsed EPR dipolar spectroscopy is a powerful tool for determining the structure and conformational dynamics of biological macromolecules, as it allows precise measurements of distances in the range of 1.5–10 nm. Utilization of high-spin Mn^{2+} species as spin probes for distance measurements is of significant interest, because they are biologically compatible and endogenous in numerous biological systems. However, to date dipolar spectroscopy experiments with this kind of species have been underexplored. Here we present pulsed electron electron double resonance (PELDOR also called DEER) and relaxation-induced dipolar modulation enhancement (RIDME) experiments, which have been performed at W-band (94 GHz) and J-band frequencies (263 GHz) on a bis-MnDOTA (DOTA = 1,4,7,10-tetraazacyclododecane-1,4,7,10-tetraacetate) model system. The distances obtained from these experiments are in good agreement with predictions. RIDME experiments reveal a significantly higher modulation depth compared to PELDOR, which is an important consideration for biological samples. These experiments also feature higher harmonics of the dipolar coupling frequency due to effective multiple-quantum relaxation of high-spin Mn^{2+} as well as the multiple-component background function. Harmonics of the dipolar coupling frequency were taken into account by including additional terms in the kernel function of Tikhonov regularization analysis.

Introduction

Pulsed electron paramagnetic resonance (EPR) dipolar spectroscopy, which can precisely measure distances in the range of 1.5–10 nm, has become a valuable tool for structural biology by providing important information about tertiary structures, conformational flexibilities and intermolecular interactions of biomacromolecules.[1–3] Pulsed electron–electron double resonance (PELDOR,[4] also called DEER[5,6]) is the most commonly used of such EPR techniques, where the distances are measured by determining the magnitude of the magnetic dipolar coupling (ω_{dd}) between pairs of spin probes, which in the weak coupling regime is given by the formula (1)[6]:

$$\omega_{dd} = \frac{\mu_B^2 g_A g_B}{\hbar} \frac{1}{R^3}\left(3\cos^2(\theta) - 1\right) = \frac{D_{dd}}{R^3}\left(3\cos^2(\theta) - 1\right) \quad (1)$$

where μ_B is the Bohr magneton, $\hbar$ is the Planck constant divided by 2π, g_A and g_B are the effective values of the g-tensor, corresponding to the excited A and B spins, R is the electron–electron distance and θ is the angle between the vector $\boldsymbol{R}$ and the external magnetic field $\boldsymbol{B}_0$. Typically such measurements are done using nitroxide radicals, which have been site-specifically attached to proteins or nucleic acid molecules.[7–11] In the last decade, paramagnetic Gd^{3+} and Mn^{2+} chelate complexes have been introduced as alternative spin probes for PELDOR spectroscopy.[12,13] Due to their high-spin multiplicities, Gd^{3+} and Mn^{2+} PELDOR measurements benefit from the use of high microwave excitation frequencies and corresponding high magnetic fields. Using high magnetic fields provides higher sensitivity, which is an important consideration for biological applications where often only a small quantity of the sample is available and spin-labelling efficiency is not 100%. Although Gd^{3+} spin-labels have been widely used for biological PELDOR applications, Mn^{2+} remains underexplored.[13–16] From the perspective of biological applications, Mn^{2+} is interesting, because many enzymes contain Mn^{2+} at their catalytic active site,[17,18] it can also readily replace diamagnetic Mg^{2+} in biological constructs[19] due to their identical charge and similarity in ionic radii.[20] These properties make EPR-based distance measurements using Mn^{2+} a potentially powerful experimental toolkit for structural biology.

Compared to nitroxide and other organic radicals, Mn^{2+} is a more complicated spin system with an electron spin of $S = 5/2$. Thus, the EPR spectrum of Mn^{2+} complexes with non-zero

[a] *Goethe-University Frankfurt am Main, Institute of Physical and Theoretical Chemistry and Center for Biomolecular Magnetic Resonance, Max von Laue Str. 7, 60438 Frankfurt am Main, Germany. E-mail: prisner@chemie.uni-frankfurt.de*
[b] *Institute for Integrative Biology of the Cell (I2BC), Department of Biochemistry, Biophysics and Structural Biology, Université Paris-Saclay, CEA, CNRS UMR 9198, Gif-sur-Yvette, F-91198, France. E-mail: sun.un@cea.fr*
[c] *Département de Chimie, Ecole Normale Supérieure, PSL Research University, UPMC Univ Paris 06, CNRS, Laboratoire des Biomolécules (LBM), 24 rue Lhomond, 75005 Paris, France*
[d] *Sorbonne Universités, UPMC Univ Paris 06, Ecole Normale Supérieure, CNRS, Laboratoire des Biomolécules (LBM), 24 rue Lhomond, 75005 Paris, France*
† Electronic supplementary information (ESI) available. See DOI: 10.1039/c6cp05239h
‡ Authors contributed equally to the work.

quadrupole Zero-Field Splitting (ZFS) parameters reveals a fine structure, consisting of five resonance lines $|m_S\rangle \rightarrow |m_S \pm 1\rangle$, where m_S is the projection of the electron spin vector to the magnetic field vector. Each of these is further split into a sextet of hyperfine lines, arising from the ^{55}Mn nuclear spin (I = 5/2, 100% abundant). In disordered samples, the total width of the EPR spectrum is defined to a large extent by the ZFS and ^{55}Mn hyperfine coupling.[21,22] The individual widths of the six hyperfine lines corresponding to the central $|-1/2,m_I\rangle \rightarrow |1/2,m_I\rangle$ transition, where m_I is the projection of the ^{55}Mn nuclear spin vector to the magnetic field vector, do not depend on ZFS in first order perturbation theory and hence these lines are very sharp. The other electron spin transitions have a first order ZFS dependency and are typically broad and featureless.

One of the important properties that governs the sensitivity of PELDOR experiments is the dipolar modulation depth. It is defined by the fraction of spins (referred to as B spins in the following) that are inverted by the applied pump pulse at the second microwave frequency, ν_B (see Fig. 1). The fraction of spins that are detected (referred to as A spins that are in resonance with the pulses at the microwave frequency of ν_A) is also an important parameter for sensitivity, since it contributes to the echo amplitude. For Mn^{2+} centers only a part of one of the six hyperfine lines of the central $|-1/2,m_I\rangle \rightarrow |1/2,m_I\rangle$ transition can be excited by the pump pulse, leading to low modulation depths of about 0.5 to 2%.[13–15,23]

As has been shown for Gd^{3+} complexes,[24,25] one way to improve on this low modulation depth condition is to use the relaxation-induced dipolar modulation enhancement (RIDME)[26,27] experiment instead of PELDOR. Unlike PELDOR, where the single-quantum electron spin transition of the B spin is driven coherently by a microwave pulse, in RIDME the B spin transition is driven incoherently by electron spin longitudinal relaxation, which is characterized by the time constant T_{1e}. Experimentally it is achieved by replacing the pump pulse at the second microwave frequency ν_B by a mixing block, composed of two $\pi/2$ pulses, applied at the detection frequency ν_A (Fig. 1).[27] In this case, the dipolar modulation depth is defined by the formula (2):

$$\lambda(T_{mix}) = \frac{1}{2}\left(1 - \exp\left(-\frac{T_{mix}}{T_{1e}}\right)\right) \quad (2)$$

where T_{mix} is the time between the two $\pi/2$ pulses in the mixing block, during which the B spin flips due to longitudinal relaxation.[27] For a dipolar-coupled spin 1/2 system the highest theoretically achievable value for the modulation depth is 50%,[27] however, as has been observed for Gd^{3+} systems, high-spin systems can achieve a larger value, due to the possibility of multiple-quantum relaxation ($\Delta m_S > 1$) of the B spin.[24] Longitudinal relaxation can drive not only single quantum transition $\Delta m_S = \pm 1$, as is the case for the spin 1/2 system, but also effectively double ($\Delta m_S = \pm 2$) and higher-quantum transitions of the B spin leading to the presence of the corresponding harmonic frequencies ($n\omega_{dd}$) in the RIDME experiments. Thus, the dipolar coupling harmonics have been observed in RIDME experiments with Gd^{3+} (ref. 24 and 25) and Mn^{2+} bis-nitroxide model compound[28] and have been attributed to the high electron spin multiplicity of the metal ion.

In the current work we describe the RIDME experiments on the bis-Mn^{2+} complex[23] shown in Fig. 2 at W-band (94 GHz, 3.3 T) and J-band (263 GHz, 9.4 T) microwave frequencies. We examined how the multiple quantum components affect the RIDME measurements and compared the performance of these experiments with PELDOR.

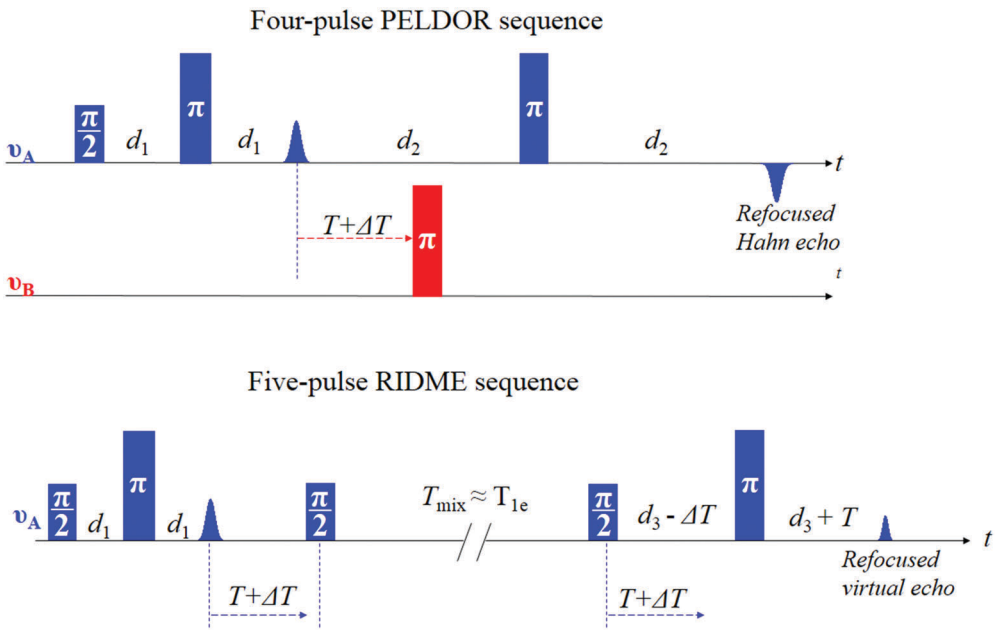

Fig. 1 Pulse schemes for the four-pulse PELDOR and five-pulse RIDME experiments.

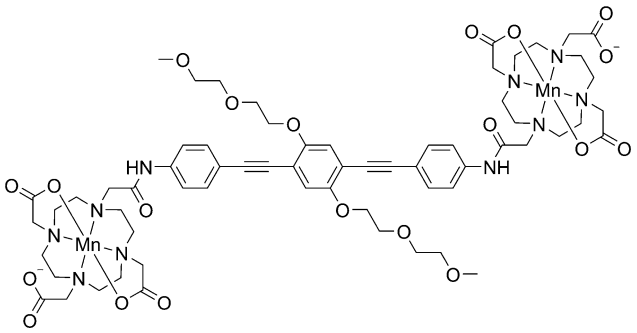

Fig. 2 The schematic chemical structure of compound **1** used in this study.

Experimental results and discussion

Pulsed EPR spectroscopy

Hahn echo-detected field-swept EPR spectrum

The field-swept Hahn echo-detected EPR spectrum of complex **1** obtained at W-band (94 GHz) frequencies is depicted in Fig. 3. It is characterized by six very narrow lines of the central $|-1/2,m_I\rangle \rightarrow |1/2,m_I\rangle$ transition of the MnDOTA complex, each separated by 252 MHz corresponding to the ^{55}Mn hyperfine coupling constant.[14] The sharpness of the lines is due to small ZFS of MnDOTA (D = 280 MHz and E = 0, each with a Gaussian distribution of 150 MHz).[14] Thus, the major contribution to the linewidth is the second and third-order perturbation terms of ZFS as well as unresolved hyperfine couplings with nitrogen and proton nuclei of the first Mn^{2+} coordination sphere. Upon increasing the microwave frequency up to the J-band (263 GHz), small narrowing of the linewidths was observed. For example, the width of the 4th hyperfine line of the central transition went from 7.7 G at 95 GHz to 6.5 G at 263 GHz. By comparison, the corresponding linewidths for molecule with a single spin-label (Fig. S1, ESI†) were 5.9 and 5.2 G. This increase in linewidth with double labelling (3.5 to 5 MHz) was due to dipolar coupling.

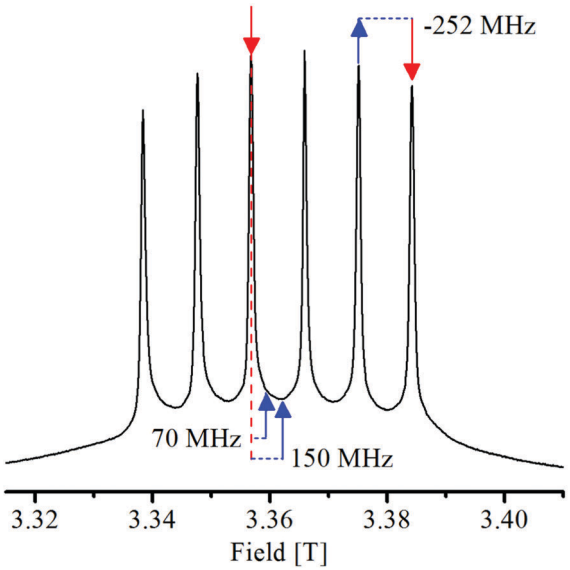

Fig. 3 The 25 K W-band field-swept Hahn echo-detected EPR spectrum of complex **1** in a deuterated solvent. The arrows indicate the resonance field positions used in the PELDOR experiments, with the red down-arrows and the blue up-arrows indicating the pump and probe positions, respectively. The pump–probe frequency offsets ($\nu_{pump} - \nu_{probe}$) are also given.

W-band (94 GHz) PELDOR experiments

W-band (94 GHz) PELDOR experiments performed on complex **1** in a deuterated solvent are shown in Fig. 4. The time traces were obtained with pump–probe pulses set at three different resonance positions in the EPR spectrum, which are shown in Fig. 3. Dipolar modulation depth of the time trace recorded with a pump–probe frequency offset of −252 MHz, corresponding to the ^{55}Mn hyperfine coupling, was smaller (1.2%) compared to the other two time traces (1.6–1.7%) due to the increased length of the pump pulse. Similar modulation depths on dipolar-coupled Mn^{2+} centers have been reported in other studies.[14,15,23] Although the modulation depth for the first case (−252 MHz offset) was about 40% smaller compared to the other two time traces, a greater sensitivity was achieved for this time trace (see Table 1, where signal-to-noise ratios (SNR) per square root of the total accumulation time are given). This is due to the fact that this PELDOR time trace was detected in resonance with the 5th hyperfine line of the central transition (see Fig. 3). As a result, the echo intensity is significantly larger, which improves the sensitivity. A further improvement of the sensitivity of such a type of PELDOR experiment can be achieved using resonators with a larger bandwidth or double-mode structures. Both have been successfully used for Gd^{3+}-based PELDOR experiments.[29,30] Another approach for increasing the sensitivity has been the use of shaped broadband pump pulses.[31–35]

The distance distributions obtained by Tikhonov regularization analysis by the DeerAnalysis[36] toolbox are shown in Fig. 4C. The most probable distances were about 2.5–2.6 nm with a full width at half maximum of about 0.6 nm for each PELDOR time trace. The distance distributions were in agreement with the structural predictions.[23]

W-(94 GHz) and J-band (263 GHz) RIDME experiments

Experimental RIDME time traces obtained at W-(94 GHz) and J-band (263 GHz) frequencies on complex **1** in protonated and deuterated solvents are shown in Fig. 5. The mixing times corresponded approximately to the T_{1e} relaxation time at 25 K for the respective frequencies. As the microwave frequency increased, the T_{1e} value shortened by a factor that was roughly equal to the ratio of microwave frequencies. Similarly, the phase memory time T_{me} also shortened upon increasing the frequency (for more details, see Sections 6 and 10 of the ESI†). Whereas no significant change to T_{1e} was found upon using a deuterated solvent, the T_{me} value lengthened, and changes to the slope of the echo decay as a function of interpulse delay were observed (see Fig. S7, S8, S31 and S32, ESI†). Thus, the mixing time at W-band frequencies was equal to 80 μs for both solvents, while at J-band frequencies the mixing times were 30 μs for the deuterated and 25 μs for the protonated solvent samples. As can be seen from Fig. 5, deuterating the solvent

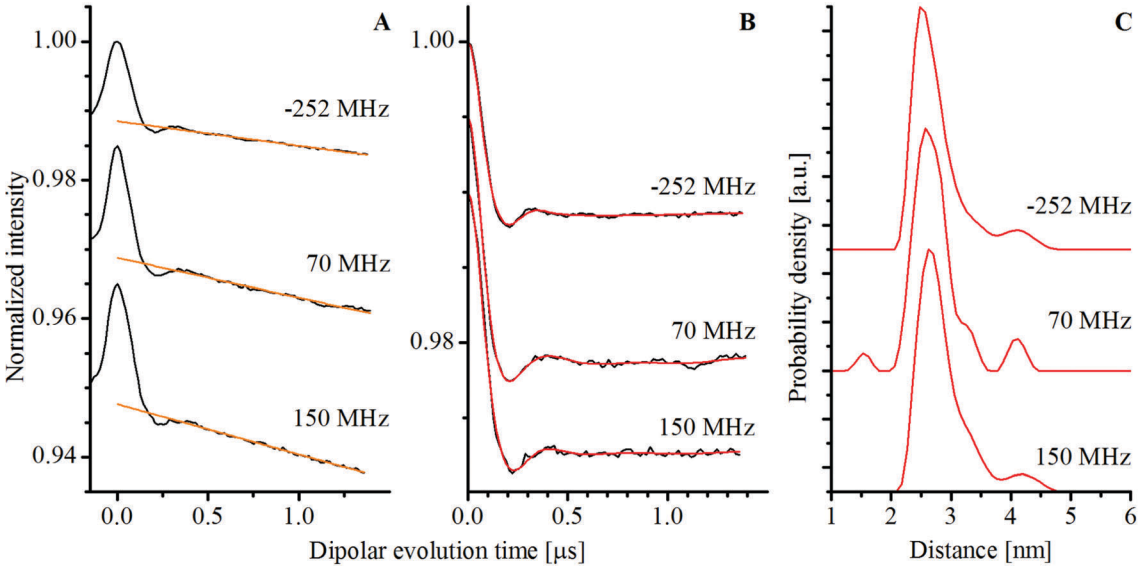

Fig. 4 The 6 K, W-band PELDOR experiments of complex **1** in a deuterated solvent, recorded at different pump–probe frequency offsets and resonance positions in the EPR spectrum (see Fig. 3). (A) The experimental time traces (black) with corresponding mono-exponential background-functions (orange). (B) The background-divided time traces (black) with corresponding fits (red) based on Tikhonov regularization analysis using a regularization parameter of 10. (C) The distance distributions obtained using Tikhonov regularization in the DeerAnalysis[36] toolbox. For better visualization, the PELDOR time traces (A and B) and distance distributions (C) have been vertically offset.

Table 1 Results of PELDOR and RIDME measurements on complex **1**

Experiment	Parameter	R_{max} [nm]	ΔR (fwhm) [nm]	λ	SNR/$\sqrt{t}$ [$h^{-0.5}$]
PELDOR	70 MHz	2.6	0.6	0.016	60
	150 MHz	2.6	0.6	0.017	50
	−252 MHz	2.5	0.6	0.012	70
RIDME	W-band, 20 μs	2.5[a]	0.6[a]	0.308	210
	W-band, 80 μs	2.6[b]	0.6[b]	0.547	150
	J-band	2.5[b]	0.6[b]	0.373	50

[a] Obtained by Tikhonov regularization with kernel function (eqn (4)). [b] Obtained by Tikhonov regularization with kernel function (eqn (5)).

influences significantly the background functions. This is related to the multiple components which contribute to the background function of RIDME. Unlike PELDOR background signals that are dominated by inter-molecular dipolar couplings, RIDME background signals additionally contain a contribution related to the transversal relaxation. In the case of a protonated solvent, the electron-nuclear spin diffusion is considerably stronger, resulting in a significantly faster decay of the RIDME signals (Fig. 5, RIDME time traces in red).

The experimental W- and J-band RIDME time traces of complex **1** in a deuterated solvent with corresponding fitted background functions (analytic functions are given in Table S1, ESI†) as well as background-divided time traces are shown in Fig. 6. The W-band time traces were obtained with two different mixing times: 20 μs corresponding roughly to 3 times T_{me} (left column, Fig. 6) and 80 μs corresponding approximately to the T_{1e} relaxation time at 94 GHz (middle column, Fig. 6). For a shorter mixing time, the dipolar modulation depth was about 30% (Fig. 6D) and for a longer mixing time it was about 55% (Fig. 6E). The experimental modulation depths were larger than the theoretical values (about 10 and 30%, respectively) obtained using eqn (2).[27] The higher experimental modulation depths might indicate the influence of the high electron spin of the Mn^{2+} ion. By comparison, the modulation depth at the J-band was about 37%, while the calculated value was about 30% (with T_{1e} of 30 μs at this frequency).

Analysis of the background-divided RIDME time traces was performed with Tikhonov regularization (see the Experimental section). The distance distributions and back-calculated dipolar evolution functions, based on the Tikhonov analysis with the conventional kernel function (identical to that used in the DeerAnalysis toolbox), given as:

$$K(T,R) = \int_0^1 \cos\left(\frac{D_{dd}}{R^3}(3x^2-1)\cdot T\right)\mathrm{d}x \qquad (3)$$

are depicted in red in Fig. 6.

The distance distributions obtained from the RIDME measurements all showed two resolved maxima rather than the one found by PELDOR. Similar complex distance distributions have been reported for RIDME experiments with Gd^{3+} ions ($S = 7/2$)[24,25] and

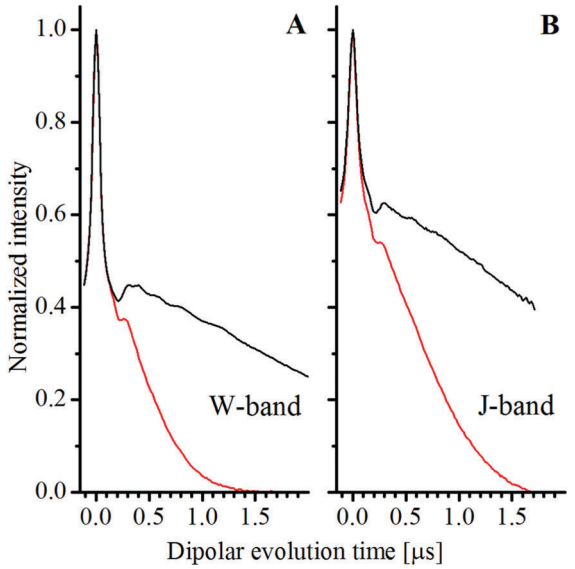

Fig. 5 The experimental RIDME time traces obtained at 25 K. (A) The traces recorded at W-band frequencies in deuterated (black) and protonated (red) solvents. (B) The traces recorded at the J-band. The mixing times were set approximately equal to the T_{1e} relaxation time of Mn^{2+} spins in the samples at the given frequency and temperature.

for the Mn^{2+} – bis-nitroxide complex.[28] This apparent increase in the complexity of the distance distributions has been attributed to multi-quantum longitudinal relaxation of high-spin systems.

The W-band RIDME time trace with a 20 μs mixing time and its analysis are depicted in Fig. 6A, D and G. The peak at about 2.5 nm obtained from Tikhonov regularization analysis with the conventional kernel function (eqn (3)) corresponded to the expected interspin distance.[23] The 2.0 nm peak corresponded to the contribution from the second harmonic of the dipolar coupling frequency. In order to test this, the second harmonic of the dipolar coupling frequency was explicitly added to the kernel function for the Tikhonov regularization:

$$K(T,R)=\int_0^1\left[\frac{1}{2}\cos\left(\frac{D_{dd}}{R^3}(3x^2-1)\cdot T\right)+\frac{1}{2}\cos\left(2\cdot\frac{D_{dd}}{R^3}(3x^2-1)\cdot T\right)\right]dx \quad (4)$$

This led to the disappearance of the 2.0 nm feature (Fig. 6G), leaving the position of the 2.5 nm peak unchanged. It was found that a weight of 0.5 for both components led to a single peak similar to the one found using PELDOR and in agreement with predictions[23] (for more detailed analysis of the dependence of the distance distributions on the weight of the $2\omega_{dd}$ component see Section 7.1 of the ESI† and Fig. S9).

The W-band RIDME time trace with a 80 μs mixing time (approximately T_{1e} at this frequency) and the analysis based on Tikhonov regularization are shown in Fig. 6B, E and H. As above, the expected 2.5 nm distance is found by Tikhonov analysis with the conventional kernel function (Fig. 6H). Assuming that the first and second harmonics of dipolar coupling frequency are equally weighted, as was the case for the experiment with a 20 μs mixing time, the peak at 2.0 nm again disappeared from the distance distribution when the modified kernel function (eqn (4)) was used (Fig. 6E and H in blue). However unlike for the measurement with a shorter mixing time, there was an additional small shoulder at about 1.8 nm in the distance distribution. To test whether this feature was due to the buildup of a triple quantum relaxation component, a kernel function having an explicit third harmonic contribution given by

$$K(T,R)=\int_0^1\left[0.425\cos\left(\frac{D_{dd}}{R^3}(3x^2-1)\cdot T\right)+0.425\cos\left(2\cdot\frac{D_{dd}}{R^3}(3x^2-1)\cdot T\right)+0.15\cos\left(3\cdot\frac{D_{dd}}{R^3}(3x^2-1)\cdot T\right)\right]dx \quad (5)$$

was used and the resulting distance distributions are shown in Fig. 6E and H in green. When the weight of the third harmonic component in the kernel function was set to 0.15 and those of the first and second harmonics to 0.425, the 1.8 nm peak disappeared (Fig. 6H and Fig. S17, ESI†) and the shape of the distance distribution more closely resembled that of the 20 μs mixing time RIDME measurements (for more detailed analysis of the dependence of the distance distribution on the weight of $2\omega_{dd}$ and $3\omega_{dd}$ components see Section 7.2 of the ESI†).

Reduced phase memory time at the J-band with respect to W-band frequencies led to a decrease in sensitivity for RIDME experiments on compound **1**. The distance distribution from the 30 μs mixing time J-band RIDME measurements using the conventional (eqn (3)) and modified kernels (eqn (4) and (5)) is shown in Fig. 6F and I (for more detailed analysis of the dependence of the distance distribution on the weight of $2\omega_{dd}$ and $3\omega_{dd}$ components see Section 7.3 of the ESI†). They were similar to the one obtained from 80 μs mixing time W-band measurements, with the most probable distance being consistent with expectations. However, Tikhonov regularization analysis using the conventional kernel function gave a wing that extended from 3 to 4 nm (red curve in Fig. 6I), which was not present in neither of the W-band RIDME measurements. Tikhonov analysis with the modified kernels (eqn (4) and (5)) enhanced the intensity of this wing (blue and green curves in Fig. 6I). A possible cause of this peak might have been the incomplete cancellation of the moving Hahn echo arising from the last two pulses (see the RIDME pulse sequence in Fig. 1) and the refocused stimulated echo due to imperfect phases of the microwave pulses in the 8-step phase cycle. The correction procedure of the J-band time trace is given in Section 8 of the ESI,† the corrected time trace and the Tikhonov regularization analysis are presented in Fig. S29 (ESI†). As can be seen from this figure, when imperfect phases are accounted for, the wing in the distance distribution was nearly completely suppressed.

It is worth noting that all three RIDME time traces had small amplitude oscillations (see Fig. 6D–F). The Fourier transforms

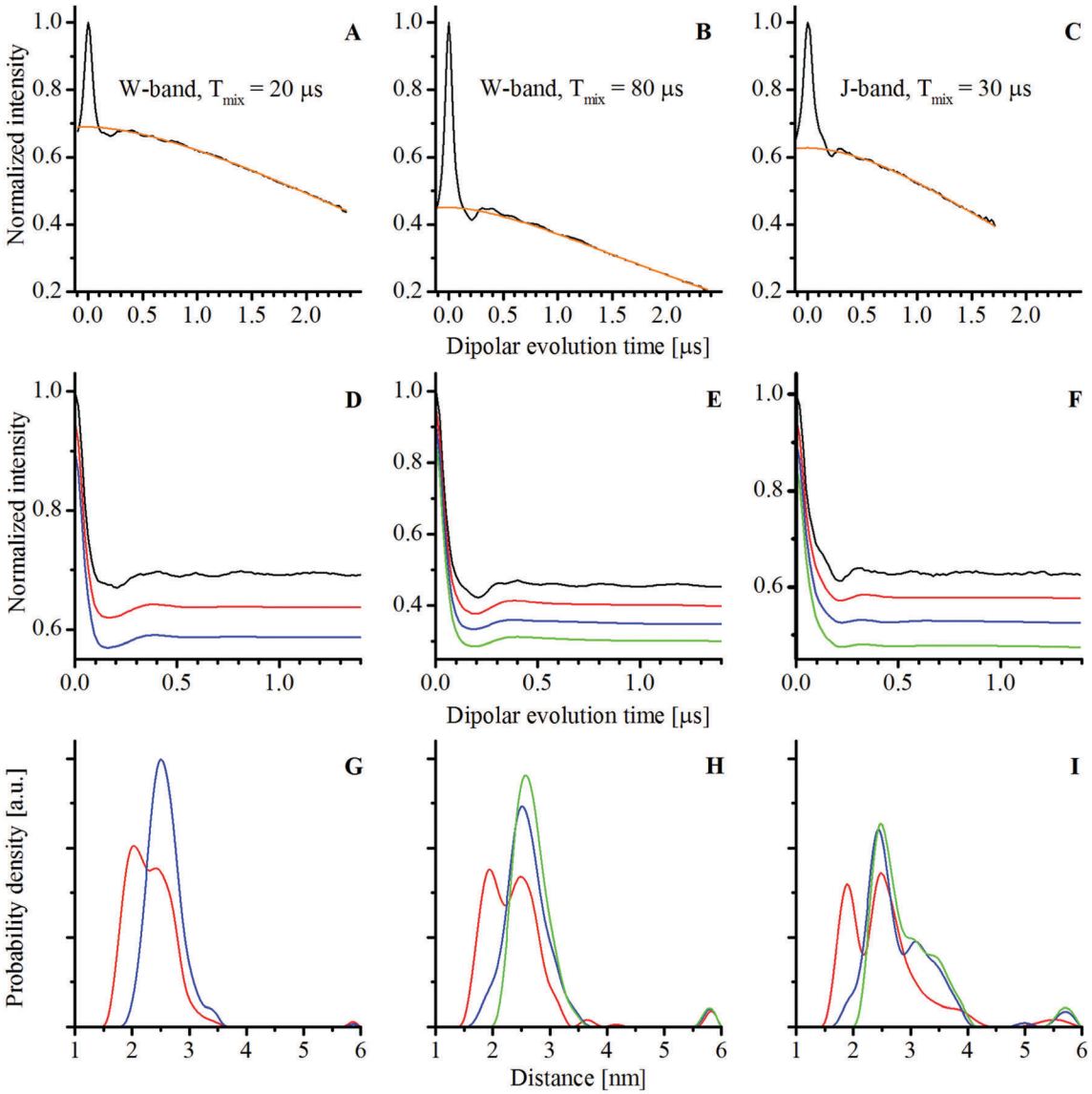

Fig. 6 The RIDME experiments in a deuterated solvent at different microwave frequencies and mixing times obtained at 25 K. (A, D and G) The experiment at W-band frequency with 20 µs mixing time. (B, E and H) The experiment at W-band frequency with 80 µs mixing time. (C, F and I) The experiment at J-band frequency with 30 µs mixing time. Detection of the RIDME signal was performed on the refocused virtual echo. (A–C) The experimental time traces (black) with corresponding stretched-exponential background functions (orange). (D–F) The background-divided experimental RIDME time traces with corresponding fits based on Tikhonov regularization analysis with standard single-frequency component kernel function (red); equally-weighted single- and double-frequency components (0.5 each) modified kernel function (blue); and equally-weighted single- and double-frequency components (0.425 each) with additional triple-frequency component (0.15) modified kernel function (green). Tikhonov regularization was performed using an in-house program with the regularization parameters set to 10 for all fitting procedures. For better visualization, the traces have been vertically offset. (G–I) The corresponding distance distributions obtained from the Tikhonov regularizations using the different kernel functions.

of the differences between the experimental RIDME time traces and back calculations revealed multiple peaks in the frequency domain (see Fig. S12, S16, S19, S24 and S27, ESI†). However, the amplitudes of these oscillations were not more than 3% of the amplitude of the dipolar oscillations. These oscillations remained when the long mixing-time W-band RIDME time trace was divided by the short mixing-time one (see Fig. S30, ESI†). This indicated that the amplitude of these oscillations built up with an increasing mixing time. A more detailed analysis of these oscillations is given in Section 7 of the ESI,† where differences in the background-divided RIDME time traces and back-calculations, based on Tikhonov analysis with different kernel functions, are shown (Fig. S11, S15, S18, S23 and S26, ESI†). Measurements on the mono-MnDOTA complex (chemical structure is shown in Fig. S1, ESI†) also had a small amplitude oscillation (see Section 5 of the ESI,† Fig. S6) but with a distinct single frequency of about 1.7 MHz. This frequency corresponded to the ^{14}N hyperfine coupling[14] and likely arose from non-coherent ESEEM effects.[37] Importantly, the oscillations seen in RIDME (Fig. 6D–F) were so small in

amplitude that they did not affect the Tikhonov analysis in any substantive way.

Comparison of PELDOR and RIDME experiments

The RIDME experiments yielded significantly larger dipolar modulation depths (up to 55%) than those obtained using PELDOR (up to 1.7%). This is a significant advantage in terms of sensitivity. The signal-to-noise ratio per square root of the total accumulation time of the RIDME and PELDOR measurements was determined in order to assess their relative efficiencies (Table 1 and see Section 15 of the ESI† for details). The RIDME measurements were up to 3 times more sensitive than the most sensitive PELDOR measurement (with −252 MHz pump–probe frequency offset), as indicated in Table 1.

However, RIDME measurements on Mn^{2+} centers have some disadvantages with respect to PELDOR. Determination of the background function for PELDOR experiments is already a non-trivial task, especially for flexible molecules, which have dipolar oscillations that dampen very quickly. But even in such cases, the PELDOR background functions have only a single component, namely inter-molecular dipolar couplings, which for randomly distributed molecules can be accurately approximated with a mono-exponential function.[4,6] By contrast, the background functions of RIDME measurements are more complex, having several different contributions which, as in previous studies,[24,25,27] appear to be adequately modeled with a stretched exponential function (analytical functions for the backgrounds are given in Table S1, ESI†). Comparisons of the RIDME and PELDOR background functions are shown in Fig. 6A–C and 4A. One can also see that the RIDME background functions strongly depend on whether the solvent is protonated or deuterated (see Fig. 4). This indicated a strong dependence on the transverse relaxation of the Mn^{2+} spin. Whereas the RIDME background definition is relatively robust in the case of a deuterated solvent (see Section 14 of the ESI† for the analysis of the influence of differently defined backgrounds on the modulation depth and the results of Tikhonov regularization analysis), a more detailed theoretical understanding of how to model the RIDME background function would be important to minimize the uncertainty in the background-correction procedure, especially for the cases where exchange of the solvent is not possible.

In contrast to PELDOR, RIDME exploits longitudinal relaxation to change the m_S state of one of the spins in the pair. In high-spin systems relaxation can effectively change m_S not only by ±1, but also by ±2 and higher. This creates additional harmonics of the dipolar coupling frequency in the experimental time trace that can be seen in the distance distribution. For model systems studied previously[24,25,28] and in this study (see Fig. 6G–I), the distance can still be precisely extracted from Tikhonov analysis with a conventional kernel function (eqn (3)). However, for more flexible systems, a not uncommon case for biomolecules, these peaks cannot be so easily distinguished. Thus, the Tikhonov analysis with the conventional kernel function can lead to the distance distribution that deviates from the real one, even assuming that the background function has been determined correctly (see Section 12 and Fig. S34 of the ESI,† where this situation is modelled). But this analysis can still be used to make an adequate estimation of the distance, since for flexible systems the distance is initially not well defined. For more precise determination of the distance the Tikhonov regularization with the modified kernel can be of interest. As can be seen from Fig. 6G–I, with this approach the unwanted contributions from the harmonics of the dipolar-coupling frequency can be removed from the distance distributions. However, the weights of the different components vary, depending on the sample and experimental conditions,[24–25,28] leading to additional parameters that must be accounted for in the data analysis. Moreover, the more complex background function of RIDME can complicate the analysis of the harmonics contributions of the dipolar coupling, as has been shown in RIDME on a protein labelled with Gd^{3+} centers.[25] Such peculiarities associated with the complex background function and harmonics of the dipolar coupling frequency in RIDME experiments with Mn^{2+} can make it difficult to obtain meaningful information particularly in flexible biological systems. However, for systems with a relatively rigid structure, where dipolar oscillations are easily seen, RIDME measurements can be quantitatively interpreted and have higher sensitivity compared to PELDOR.

These considerations suggest that Mn^{2+} – based RIDME measurements are best suited for cases where accurate distances are not required, for example for determining the quaternary structures of proteins or for optimizing labelling conditions. Such applications can be performed more quickly due to the higher sensitivity and relative simplicity of setting up the RIDME experiment. For the cases where accurate distances are needed, RIDME can be complemented with PELDOR, which requires longer measurement times.

Experimental

The concentration of compound **1** was 50 μM in D_2O : glycerol-d_8 or H_2O : glycerol, 4 : 1, v : v with 100 mM HEPES at pD or pH 8. The detailed synthesis of the compound and initial characterization are presented in another study.[23] RIDME and PELDOR experiments were performed in a deuterated solvent with the exception of some RIDME time traces shown in Fig. 4.

W-band pulsed EPR measurements

Pulsed EPR experiments at W-band frequencies were performed on a Bruker Elexsys E680 EPR spectrometer, equipped with a Bruker ''power upgrade 2'' and an Oxford Instruments CF935 flow cryostat. The Hahn echo-detected field-swept EPR spectrum was obtained with 10 and 20 ns pulses, an interpulse delay of 400 ns, 1 shot per point, a pulse repetition time of 11 ms, a sweep width of 0.1 T at a temperature of 25 K.

All RIDME experiments were performed with a deadtime-free five pulse sequence at a sample temperature of 25 K.[27]

The W-band RIDME experiment with a mixing time of 20 μs was conducted with 10 ns and 20 ns π/2 and π pulses, respectively. This short mixing time was about $3T_{me}$ time in order to eliminate the transversal component of the

magnetization. Hence, the unnecessary echo signals originating from the π/2 pulses of the mixing block and other pulses in the sequence, and, therefore, distortions in the RIDME time traces, are removed. Initial delay between pulses (d_1 in Fig. 1) was 400 ns. The initial time position for the mixing block (position of the first π/2 pulse in the block) was 300 ns after the first π pulse. The time delay between the second π/2 in the block and the last π pulse (d_3 in Fig. 1) was 2.5 μs. The sequence can be represented: 10 ns-400 ns-20 ns-(300 ns + ΔT)-10 ns-20μs-10 ns-(2.5 μs − ΔT)-20 ns-2.4 μs-echo. The time increment ΔT was 16 ns with 156 number of points. A shot repetition time was 1 ms and the number of shots per point was 100. The 8-step phase cycle protocol[27] for the π/2 pulses was used. 55 scans were taken corresponding to a total accumulation time of about 2 hours. For the RIDME experiments with a mixing time of 80 μs on compound **1** in a deuterated solvent, 371 scans were taken corresponding to a total accumulation time of about 14.23 hours. For analogous measurements in a protonated solvent, 507 scans were taken corresponding to a total accumulation time of about 16 hours. All W-band RIDME measurements were performed with the resonance position of the pulses set to the highest field hyperfine line of the central transition.

W-band PELDOR measurements were performed at 6 K using the standard four-pulse, deadtime-free PELDOR/DEER sequence,[1,6] with a four-step two-phase cycle.[38] The initial interpulse delay (between detection π/2 and π pulses) was 544 ns and the dipolar evolution window was 2226 ns. The initial time delay between the detection π pulse and the pump pulse was 364 ns which was incremented by 16 ns with 100 number of points. The shot repetition time was 800 μs with 100 shots per point. For measurements with a pump–probe frequency offset of 70 MHz, the pump pulse duration was 24 ns and the duration of the π/2 and π detection pulses was 12 and 24 ns. The number of scans was 256 resulting in a total accumulation time of about 2.34 hours. For measurements with a pump–probe frequency offset of 150 MHz, the pump pulse duration was 24 ns and the duration of the π/2 and π detection pulses was 36 and 72 ns. The number of scans was 363 resulting a total accumulation time of about 3.32 hours. For measurements with a pump–probe frequency offset of −252 MHz, the pump pulse duration was 58 ns and the duration of the π/2 and π detection pulses was 30 and 58 ns. The number of scans was 243 resulting in a total accumulation time of about 2.22 hours.

J-band pulsed EPR measurements

J-band RIDME experiments were performed on a 263 GHz Bruker Elexsys E780 pulsed EPR spectrometer. The system is equipped with a 9.4 T superconducting magnet, with a quasi-optical front-end with a microwave power of about 15 mW and an arbitrary waveform generator (AWG). The J-band RIDME experiment with a mixing time of 30 μs was conducted with 18 ns and 32 ns π/2 and π pulses, respectively. Initial delay between pulses (d_1 in Fig. 1) was 400 ns. The initial time position for the mixing block (the position of the first π/2 pulse in the block) was 300 ns after the first π pulse. The time delay between the second π/2 in the block and the last π pulse (d_3 in Fig. 1) was 2.0 μs. The sequence can be represented: 18 ns-400 ns-32 ns-(300 ns + ΔT)-18 ns-30 μs-18 ns-(2.0 μs − ΔT)-32 ns-1.9 μs-echo. The time increment ΔT was 16 ns with 115 number of points. The shot repetition time was 0.5 ms and the number of shots per point was 100. A 8-step phase cycle protocol[27] for the π/2 pulses was used. 930 scans were taken corresponding to a total accumulation time of about 12.95 hours.

The J-band RIDME time trace on compound **1** in a protonated solvent (Fig. 4) was obtained with 16 ns and 30 ns π/2 and π pulses, respectively, and a mixing time of 25 μs. All the other parameters were identical to those in the previous case. The number of scans was 1133 resulting to a total acquisition time of about 18 hours. All J-band RIDME time traces were obtained with the resonance position of the pulses set to the lowest field hyperfine line of the central transition. No change in the time traces upon changing the resonance position of the pulses to the highest field hyperfine line was observed.

Tikhonov regularization analysis

The Tikhonov program used in our analysis closely followed the one found in DeerAnalysis.[36] This implementation was faster and more flexible with regard to the use of non-conventional kernels. Our implementation was validated by comparing the results against those obtained using DeerAnalysis for a set of PELDOR measurements.

Our Fortran-90 program was an adaption of the program FTIKREG[39] which minimizes a functional:

$$G(P) = \|KP - F\|^2 + \lambda\|LP\|, \quad (6)$$

where

$$F(T) = K(T,R)P(R) \quad (7)$$

and for PELDOR measurements, as described previously,[36] $F(T)$ is the PELDOR form factor, $P(R)$ is the distance distribution and $K(T,R)$ is the kernel function. The conventional kernel function that was used was identical to that used in DeerAnalysis.[36,40] L was the second derivative operator. Although provided as an option in FTIKREG, $P(R)$ was always constrained to be positive in our implementation.[36] Low-level linear algebra routines (*e.g.* SVD) in the original FTIKREG were replaced with appropriate optimized operating system libraries. The ''self-consistency'' method of FTIKREG was not implemented since it has been shown previously that the L-curve graphical solution method was more appropriate.[36,41] Based on the visual inspection of the Tikhonov solutions and L-curves (see above), a regularization parameter of 10 was found to be appropriate for the reported measurements.

Conclusion

RIDME and PELDOR experiments were performed on a model compound, containing two dipolar-coupled Mn^{2+} ions. RIDME experiments were performed at W- and J-band microwave frequencies. For the studied system, where the ligand for Mn^{2+} ion is DOTA, it is advantageous to perform the experiments at W-band

frequency, due to a higher electron spin phase memory time at this frequency. A significant influence of the solvent deuteration on the background function was observed for RIDME experiments at both frequencies.

Both types of EPR dipolar spectroscopy experiments, RIDME and PELDOR, yielded a distance of 2.5–2.6 nm in good agreement with predictions. RIDME gave a significantly larger modulation depth (up to 55%) with respect to PELDOR (up to 1.7%) that led to a significant gain in sensitivity. In general, RIDME is instrumentationally less demanding than PELDOR, since it does not require a second microwave frequency and an associated increased spectrometer bandwidth. The complex background function and contributions from harmonics of the dipolar coupling frequency can reduce the accuracy of distances determined using RIDME especially in cases where systems are flexible. The harmonic contributions can be accounted for by using a kernel that includes such terms in the Tikhonov analysis, but at the price of increased complexity in interpretation. Based on this, we concluded that the RIDME technique is best suited for the quantitative analysis of relatively rigid systems or cases where accurate distances are less important and sensitivity is of highest priority.

Acknowledgements

This work was supported by a joint ANR/DFG project (MnHFPELDOR, ANR-DFG Chemistry 2011-INTB-1010-01) and DFG (PR 294/14-1), the French Infrastructure for Integrated Structural Biology (FRISBI, ANR-10-INSB-05-01), the CNRS "Interface PCB" program, the DFG Priority Program 1601 (New Frontiers in Sensitivity for EPR Spectroscopy). The W-band EPR spectrometer was funded by the Region Ile-de-France "Sesame" program, the CEA, and CNRS and the J-band EPR spectrometer by the Cluster of Excellence Frankfurt (CEF) Macromolecular Complexes.

References

1 M. Pannier, S. Veit, A. Godt, G. Jeschke and H. W. Spiess, *J. Magn. Reson.*, 2000, **142**, 331.
2 G. Jeschke, *Annu. Rev. Phys. Chem.*, 2012, **63**, 419.
3 O. Schiemann and T. F. Prisner, *Q. Rev. Biophys.*, 2007, **40**, 1.
4 A. D. Milov, K. M. Salikhov and M. D. Shchirov, *Phys. Solid State*, 1981, **23**, 565.
5 R. G. Larsen and D. J. Singel, *J. Chem. Phys.*, 1993, **98**, 5134.
6 R. E. Martin, M. Pannier, F. Diederich, V. Gramlich, M. Hubrich and H. W. Spiess, *Angew. Chem., Int. Ed.*, 1998, **37**, 2833.
7 W. L. Hubbell, A. Gross, R. Langen and M. Lietzow, *Curr. Opin. Struct. Biol.*, 1998, **8**, 649.
8 W. L. Hubbell, C. J. López, C. Altenbach and Z. Yang, *Curr. Opin. Struct. Biol.*, 2013, **23**, 725.
9 G. E. Fanucci and D. S. Cafiso, *Curr. Opin. Struct. Biol.*, 2006, **16**, 644.
10 I. Krstic, B. Endeward, D. Margraf, A. Marko and T. F. Prisner, *Top. Curr. Chem.*, 2012, **321**, 159.
11 S. A. Shelke and T. T. Sigurdsson, *Eur. J. Org. Chem.*, 2012, 2291.
12 A. Raitsimring, C. Gunanathan, A. Potapov, I. Efremenko, J. Martin, D. Milstein and D. Goldfarb, *J. Am. Chem. Soc.*, 2007, **129**, 14138.
13 D. Banerjee, H. Yagi, T. Huber, G. Otting and D. Goldfarb, *J. Phys. Chem. Lett.*, 2012, **3**, 157.
14 H. Y. V. Ching, P. Demay-Drouhard, H. C. Bertrand, C. Policar, L. C. Tabares and S. Un, *Phys. Chem. Chem. Phys.*, 2015, **17**, 23368.
15 A. Martorana, Y. Yang, Y. Zhao, Q.-F. Li, X.-C. Su and D. Goldfarb, *Dalton Trans.*, 2015, **44**, 20812.
16 H. Y. V. Ching, F. C. Mascali, H. C. Bertrand, E. M. Bruch, P. Demay-Drouhard, R. M. Rasia, C. Policar, L. C. Tabares and S. Un, *J. Phys. Chem. Lett.*, 2016, **7**, 1072.
17 K. Wieghardt, *Angew. Chem., Int. Ed.*, 1989, **28**, 1153.
18 G. Reed and G. Markham, in *Biological Magnetic Resonance*, ed. L. Berliner and J. Reuben, 1984, vol. 6, p. 73.
19 T. Schweins, K. Scheffzek, R. Aßheuer and A. Wittinghofer, *J. Mol. Biol.*, 1997, **266**, 847.
20 C. W. Bock, A. K. Katz, G. D. Markham and J. P. Glusker, *J. Am. Chem. Soc.*, 1999, **121**, 7360.
21 G. L. Bir and L. S. Sochava, *Phys. Solid State*, 1964, **5**, 2637.
22 G. L. Bir, *Phys. Solid State*, 1964, **5**, 1628.
23 P. Demay-Drouhard, H. Y. V. Ching, D. Akhmetzyanov, R. Guillot, L. C. Tabares, H. C. Bertrand and C. Policar, *ChemPhysChem*, 2016, **17**, 2066.
24 S. Razzaghi, M. Qi, A. I. Nalepa, A. Godt, G. Jeschke, A. Savitsky and M. Yulikov, *J. Phys. Chem. Lett.*, 2014, **5**, 3970.
25 A. Collauto, V. Frydman, M. D. Lee, E. H. Abdelkader, A. Feintuch, J. D. Swarbrick, B. Graham, G. Otting and D. Goldfarb, *Phys. Chem. Chem. Phys.*, 2016, **18**, 19037.
26 L. V. Kulik, S. Dzuba, I. Grigoryev and Y. D. Tsvetkov, *Chem. Phys. Lett.*, 2001, **343**, 315.
27 S. Milikisyants, F. Scarpelli, M. G. Finiguerra, M. Ubbink and M. Huber, *J. Magn. Reson.*, 2009, **201**, 48.
28 A. Meyer and O. Schiemann, *J. Phys. Chem. A*, 2016, **120**, 3463.
29 I. Kaminker, I. Tkach, N. Manukovsky, T. Huber, H. Yagi, G. Otting, M. Bennati and D. Goldfarb, *J. Magn. Reson.*, 2013, **227**, 66.
30 M. R. Cohen, V. Frydman, P. Milko, M. Iron, E. H. Abdelkader, M. D. Lee, J. D. Swarbrick, A. Raitsimring, G. Otting, B. Graham, A. Feintuch and D. Goldfarb, *Phys. Chem. Chem. Phys.*, 2016, **18**, 12847.
31 P. E. Spindler, S. J. Glaser, T. E. Skinner and T. F. Prisner, *Angew. Chem., Int. Ed.*, 2013, **52**, 3425.
32 A. Doll, S. Pribitzer, R. Tschaggelar and G. Jeschke, *J. Magn. Reson.*, 2013, **230**, 27.
33 A. Doll, M. Qi, N. Wili, S. Pribitzer, A. Godt and G. Jeschke, *J. Magn. Reson.*, 2015, **259**, 153.
34 A. Doll, M. Qi, S. Pribitzer, N. Wili, M. Yulikov, A. Godt and G. Jeschke, *Phys. Chem. Chem. Phys.*, 2015, **17**, 7334.
35 P. E. Spindler, I. Waclawska, B. Endeward, J. Plackmeyer, C. Ziegler and T. F. Prisner, *J. Phys. Chem. Lett.*, 2015, **6**, 4331.
36 G. Jeschke, V. Chechik, P. Ionita, A. Godt, H. Zimmermann, J. Banham, C. Timmel, D. Hilger and H. Jung, *Appl. Magn. Reson.*, 2006, **30**, 473.

37 L. V. Kulik, E. S. Salnikov and S. Dzuba, *Appl. Magn. Reson.*, 2005, **28**, 1.
38 E. Matalon, T. Huber, G. Hagelueken, B. Graham, V. Frydman, A. Feintuch, G. Otting and D. Goldfarb, *Angew. Chem., Int. Ed.*, 2013, **52**, 11831.
39 J. Weese, *Comput. Phys. Commun.*, 1992, **69**, 99.
40 G. Jeschke, G. Panek, A. Godt, A. Bender and H. Paulsen, *Appl. Magn. Reson.*, 2004, **26**, 223.
41 Y.-W. Chiang, P. P. Borbat and J. H. Freed, *J. Magn. Reson.*, 2005, **172**, 279.

